Dynamics of Glial Cell Defense Mechanisms in Response to Ischemic Hypoxia in the Brain

Matthew Buhr[1], Oscar Garcia[2], Tiffany Reyes[3], Hasan Sumdani[4], Kamal Barley [5], Adrian Smith[5], Benjamin Morin[6], Anuj Mubayi[7]

[1] Department of Mathematics, University of South Dakota, Vermillion, South Dakota
[2] School of Physics, Universidad de Costa Rica, San José, Costa Rica
[3] Department of Mathematics, Whittier College, Whittier, California
[4] Department of Biology, University of Texas at Arlington, Arlington, Texas
[5] Applied Mathematics for the Life and Social Sciences, Arizona State University, Tempe, Arizona
[6] Global Institute of Sustainability, Arizona State University, Tempe, Arizona
[7] Simon A. Levin Mathematical, Computational and Modeling Sciences Center, Tempe, Arizona

Abstract

Three models are introduced that explore the dual role of glial cells in the formation of scar tissue and in the neural repair following hypoxia ischemia in the brain. Scar tissue helps protect the brain during the acute phase of injury by limiting the spread of secondary damage, but limits recovery by inhibiting the repair of damaged neurons. Scar formation is not ideal, however repaired neurons are still susceptible to damage and do nothing to halt the spread of ischemic injury. A stochastic, spatially explicit Cellular Automaton (CA) model is used to capture the dynamics of neural tissue repair and the containment of damage by scar tissue. In addition, two deterministic models are developed to approximate the stochastic process namely, Mean Field (MFA) and Pair Approximation (OPA) models. We show that the MFA neglects all spatial dependence among state variables. The OPA models the dynamics of state variables evolving as pairs, where spatial adjacency matters. Our results compare how the trade-off between scar tissue formation and neural repair impacts future brain health.

1 Introduction

Strokes rank as 4th among all causes of death [5]. Ischemic strokes are sometimes called "brain attacks" because they are caused by clots that obstruct oxygen's flow to the brain (similar to how a heart attack deprives the heart of oxygen). This leaves the downstream cells susceptible to damage due to lack of oxygen. Significant brain damage can occur following a stroke due to rapid cell damage. Additionally, the occurrence of secondary cell damage may follow a hypoxic (oxygen deprived) episode [3]. This process of secondary cell damage is the one we focus on and is currently understood to be rooted in the change in cellular metabolism following a prolonged period of hypoxia. After aerobic (oxygenated) conditions are restored to the brain, the actions of the mitochondrion organelle (a cellular subunit) in affected cells are impacted. Modifications in metabolic pathways related to energy retrieval from glucose by the mitochondrion lead to shifts in relative concentrations of metabolites (by-products of metabolism). The resulting degeneration of mitochondria gives rise to cell-damaging chemicals in the cytosol (the intracellular fluid) which would not be present otherwise because they are normally stored in the intermembrane space of the mitochondrion [11].

This secondary phase in cell damage is less rapid than the acute phase of stroke and typically occurs in such a way that cells closest to affected cells are most susceptible to further damage [3]. This implies that there is a spatial dependence (biologically explained by gap junctions–channels that connect cells). Due to the frequent intercellular gap junction connections, biochemical signals can be relayed to nearby cells promoting a chain reaction of cell damage to areas near cells that have already been damaged by the clot [11].

Connexin 43 (a type of gap junction) gives a route for which damaging biochemical signals

from one cell can be effective for spurring damage of additional cells that are closeby. Activation of connexin 43 has also been postulated to trigger events that lead to the formation of glial scars (neural scar tissue) [6], one of the two defensive mechanisms that we model, which takes place in the brain to prevent further damage. Glial scars are produced by glial cells which are present in the brain as supportive cells for neurons (the cells which communicate via electrical and chemical impulses). Glial cells interact with damaged cells to make the glial scar.

The formation of the glial scar involves multiple types of glial cells. For instance, microglia (a type of glial cell) help with scar formation by consuming dead and damaged cells, which provides ample space in the central nervous system for formation of scar tissue. Once space has been provided by the actions of the microglia, astrocytes (another type of glial cell) in the penumbra (the viable area surrounding the oxygen-deprived region) become reactive and protract their cellular extensions to create a physical barrier between injured and non-injured tissues [9].

Glial scars provide protection of neural tissue by forming barriers to stop the spread of damage following a mild traumatic brain injury, but the scar tissue can also be detrimental because it blocks healthy neurons from proliferating and making new neural connections after the same traumatic event [9]. In the context of this study, glial scars can be thought of as blockers of the cell-damage chemicals that are released by degenerating mitochondria after a hypoxic event occurs. In this way, the newly created glial scar can limit the extent of neuron damage by protecting healthy cells from the paracrine (local cell communication) signals of damaged cells [9].

Despite the utility of a glial scar during times of spreading injury, the glial scar serves little purpose after the spread has ceased. It is possible that promoting other glial cell actions, such as neuron repair, can help with functional recovery after an injury [8]. Neural reparation is the second

action of glial cells that we model in this study. Reclamation of damaged cells in the penumbra may occur only if they have not become permanently inviable (a classifcation of damaged cells we do not consider here) [4]. While it may seem most beneficial for glial cells to only repair neurons after an injury, rather than form scar tissue, repaired neurons offer no protection from the spreading damage, therefore repaired neurons still carry a risk of becoming damaged again.

We note that a trade-off exists between glial scar formation and neural repair: an excess amount of scarring can help protect the brain from more damage occurring, but only after sacrificing brain function; while a smaller amount of scar formation can allow for more neural repair, but risks more injury from the initial amount of damage. In our study we focus on this trade-off: What balance of scar formation and neural repair will contain damage effectively without compromising functionality? To answer this we employ several mathematical modeling methods: Cellular Automaton (CA), Mean Field (MFA), and Pair Approximation (OPA). These methods give a comprehensive view of the trade-offs between the two different glial cell activities we study during the recovery period following hypoxia. Each model uses unique methods, therefore the information predicted by each one provides a distinct view of the recovery process.

We begin with the stochastic CA model because we believe that its spatial explicitness offers the best representation of the biology [2]. From the rules used to formulate CA we then derive MFA whose spatial independence allows us to perform intricate mathematical analysis. Although this is a drawback considering the highly spatial nature of the biological question, the mean field's independence from spatial considerations makes it the simplest of our three models, therefore allowing the most detailed analysis. From MFA we move on to OPA which is deterministic like MFA, but incorporates a degree of spatial dependence by considering pairs instead of individual

states.

To conclude our study, we conduct parameter sweeps of the rates of scar cell formation and neural reparation with respect to equilibrium values of our state variables. We also consider the effects of alternate initial proportions of glial cells.

2 Mathematical Models

In our mathematical models, we define four states: healthy(H), damaged(D), glial(G), and scar cells(S).

Table 1: State Variables & Parameters

State	Meaning
H	Healthy cells
D	Damaged cells
G	Glial cells
S	Scar cells
Parameter	**Definition**
θ	Rate of scar cell formation
τ	Rate of damaged cell reparation
γ	Rate of damage to healthy cells

Healthy cells are functioning neurons that can be damaged due to contact with damaged cells at rate γ. Damaged cells are weakened (non-functional) cells that will remain damaged unless acted upon by glial cells which either repair them to form healthy cells at rate τ or form scar cells at rate θ. Scar cells are static; they only offer protection to other cells by containing the damage caused by trauma. From these biological processes, we can describe the transition rules:

$$\text{H interacts with D} \xrightarrow{\gamma} \text{H becomes D}$$

$$\text{G interacts with D} \xrightarrow{\tau} \text{D becomes H}$$

$$\text{G interacts with D} \xrightarrow{\theta} \text{both G and D become S}$$

3 Cellular Automaton Model

The interactions that occur after the stroke are spatially explicit, which means that cells have to be adjacent to interact. We chose the Cellular Automaton (CA) model to be our *in silico* representation of the system's biology. We use toroidal boundary conditions (see Figure 1) to simulate an infinite lattice, which is necessary to prevent false encapsulation effect over the damage (a cell is encapsulated against a wall). Also, we used this setting to avoid using more complex boundaries, ranging from reflecting to absorbing boundaries.

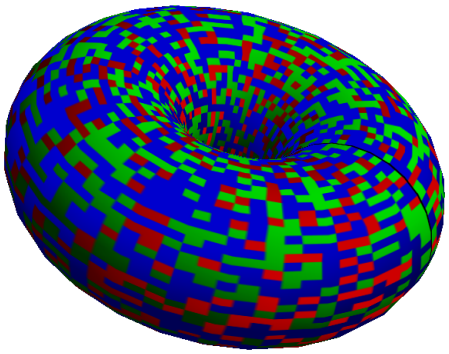

Figure 1: Representation of boundary conditions

In the 100x100 CA we use, each cell only interacts with their cardinal neighbors (the von Neumann neighborhood) via the events described earlier. The CA is initialized with zero scar cells and with a random distribution of healthy and glial cells. While the random distribution of healthy and glial cells is assumed, three cases of the distribution of damaged cells are considered: randomly

distributed, completely clustered (circular spot) and clustered with random non-damaged spots. All random processes were implemented using uniformly distributed random variables. For the later two cases, we chose the size of the damage to be small enough to prevent self-intersection through the boundary conditions. The damage can therefore only expand and interact with itself locally. This assumption matches biological observations, in which the ischemic primary damage is on average 10% of the cerebral volume [10].

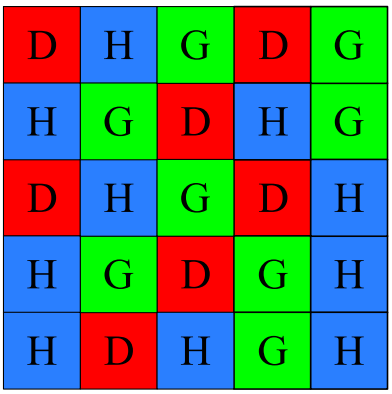

Figure 2: An example of a section of the Cellular Automaton lattice.

Our CA model is a continuous-time Poisson Process[7] and its time evolution is dictated by the Gillespie algorithm. This means that only one event may happen at any given time and that time is an exponentially distributed random variable with intensity R_T[1], which is the total rate at which any event may occur. R_T and the probabilities for the events to ocurr are given by:

$$R_T = \gamma P[HD]N_P + (\theta + \tau)P[GD]N_P \quad (1)$$

$$P_{HD\to DD} = \frac{\gamma P[HD]N_P}{R_T} \quad (2)$$

$$P_{GD\to GH} = \frac{\tau P[GD]N_P}{R_T} \quad (3)$$

$$P_{GD\to SS} = \frac{\theta P[GD]N_P}{R_T} \quad (4)$$

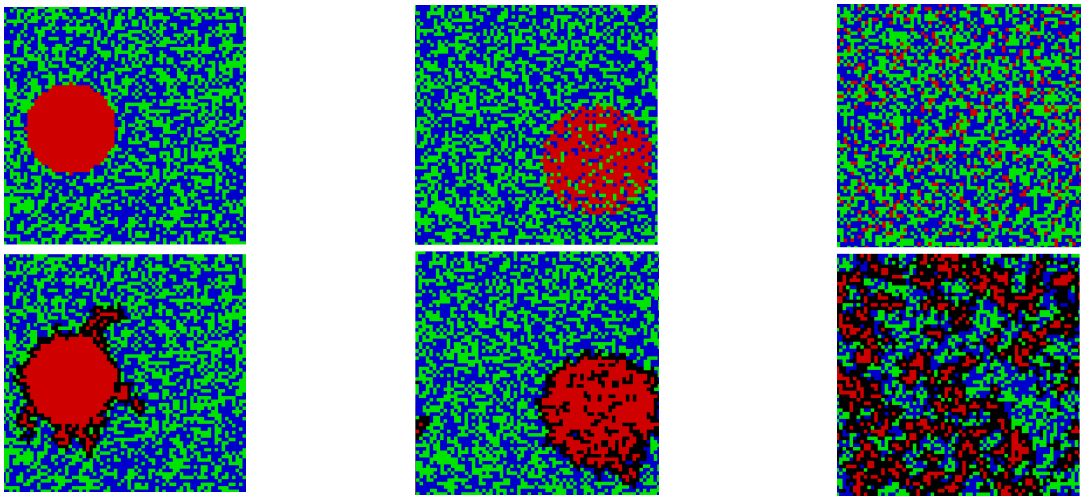

Figure 3: CA realizations at initial state (top) and steady state (bottom) with clustered (left), semi-clustered (middle), and random (right) initial damage

Where N_p is the total number of existing pairs, and $P[HD]$ is the proportion of HD pairs, for example. One event is randomly chosen based on this distribution, and an appropriate cell for the given event is randomly chosen from the lattice. This cell interacts randomly with one of its neighbors, depending on the rule chosen. The stochastic process reaches steady state when $R_T(t)$ is less than one thousandth of the initial total rate. The ratio of the initial and final rates was chosen relative to the total number of cells. For demonstrations of the CA realization in all initial damage conditions see Figure 3.

4 Mean Field Model

The Mean Field model (MFA) offers a deterministic interpretation of healthy, damaged, glial, and scar cell interaction post ischemic stroke. In the event of hypoxia, cells near the obstructed blood vessel are affected, while cells more distant to the obstruction are affected less or not at all. The mean field model's simplicity allows for thorough mathematical analysis. However, it does

not take into account any type of spatial interaction/dependence. Due to the spatially dependent interactions of the cells, the mean field model is limited in appropriately depicting the biology. Our system of ordinary differential equations is as follows (with the state variables and parameters defined in Table 1):

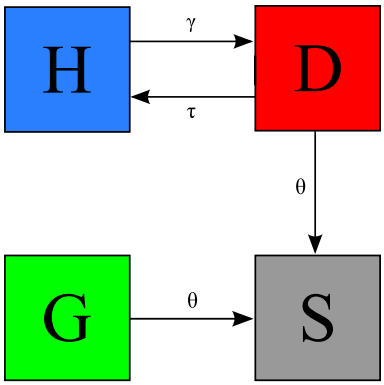

Figure 4: Flow diagram of the MFA

$$\frac{d}{dt}\mathcal{P}[H] = \tau\mathcal{P}[G]\mathcal{P}[D] - \gamma\mathcal{P}[H]\mathcal{P}[D] \tag{5}$$

$$\frac{d}{dt}\mathcal{P}[D] = -\theta\mathcal{P}[G]\mathcal{P}[D] - \tau\mathcal{P}[G]\mathcal{P}[D] + \gamma\mathcal{P}[H]\mathcal{P}[D] \tag{6}$$

$$\frac{d}{dt}\mathcal{P}[G] = -\theta\mathcal{P}[G]\mathcal{P}[D] \tag{7}$$

$$\frac{d}{dt}\mathcal{P}[S] = 2\theta\mathcal{P}[G]\mathcal{P}[D] \tag{8}$$

The change in the proportion of healthy cells is shown by equation 5 and is moderated by two events. Damaged cells recover after interacting with glial cells at rate τ, while healthy cells become damaged after interacting with damaged cells at rate γ.

The change in the proportion of damaged cells is represented by equation 6 and includes three events. Healthy cells become damaged after interacting with damaged cells at rate γ. Damaged

cells become either healthy or scarred after interacting with glial cells at rates τ or θ respectively.

The change in the proportion of glial cells in the system is represented by equation 7 and is affected by one event. The proportion of glial cells decreases as they interact with damaged cells and turn into scar cells at rate θ. This interaction turns both the damaged and glial cells into scar cells (the rationale behind the presence of the factor 2 in the differential equation for scar cells). The states and the appropriate biological events that they undergo are shown in Figure 4.

From the Law of Total Probability and the form of equations 7 and 8, we obtain the following invariants of motion:

$$\mathcal{P}[H] + \mathcal{P}[D] + \mathcal{P}[G] + \mathcal{P}[S] = 1, \tag{9}$$

$$2\left(\frac{d\mathcal{P}[G]}{dt}\right) + \frac{d\mathcal{P}[S]}{dt} = 0. \tag{10}$$

From equation 10 we derive the following equivalent expression:

$$2\mathcal{P}[G] + \mathcal{P}[S] = k \mid k \in \mathbb{R}. \tag{11}$$

Using equations 9 and 11 we obtain:

$$\mathcal{P}[G] = \mathcal{P}[H] + \mathcal{P}[D] + k - 1. \tag{12}$$

Equation 12 can be substituted into equations 5 and 6, simplifying our system to two dimensions.

$$\frac{d}{dt}\mathcal{P}[H] = \mathcal{P}[D](\tau(\mathcal{P}[H] + \mathcal{P}[D] + k - 1) - \gamma\mathcal{P}[H]). \tag{13}$$

$$\frac{d}{dt}\mathcal{P}[D] = \mathcal{P}[D](\gamma\mathcal{P}[H] - (\theta + \tau)(\mathcal{P}[H] + \mathcal{P}[D] + k - 1)). \tag{14}$$

There is one isolated fixed point and a line of non-isolated equilibria given by $(H_\infty, D_\infty) = (0, 1-k)$ and $(H_\infty, D_\infty) = (H^*, 0)$ respectively. The following local stability analysis is one case of our equilibrium line. See Appendix A for a full stability analysis of $(H_\infty, D_\infty) = (H_\infty, 0)$. Stability

analysis of the isolated fixed point $(0, 1-k)$ follows.

4.1 Local Stability Analysis of Damage-Free Equilibria

In order analyze the stability of the non-isolated line of equilibria, $(H_\infty, D_\infty) = (H_\infty, 0)$, we calculate the Jacobian matrix given our 2-dimensional system of equations:

$$J(\mathcal{P}[H], \mathcal{P}[D]) = \begin{bmatrix} (\tau-\gamma)\mathcal{P}[D] & \tau(\mathcal{P}[H]+2\mathcal{P}[D]+k-1)-\gamma\mathcal{P}[H] \\ (\gamma-\theta-\tau)\mathcal{P}[D] & \gamma\mathcal{P}[H]-(\theta+\tau)(\mathcal{P}[H]+2\mathcal{P}[D]+k-1) \end{bmatrix}.$$

We evaluate the Jacobian matrix at $(H_\infty, D_\infty) = (H_\infty, 0)$:

$$J(H^*, 0) = \begin{bmatrix} 0 & \tau(1-k)+(\tau-\gamma)H_\infty \\ 0 & (\theta+\tau)(1-k)+(\gamma-\theta-\tau)H_\infty \end{bmatrix}.$$

This matrix produces the following eigenvalues λ_1 and λ_2:

$$\lambda_1 = 0,$$

$$\lambda_2 = (\theta+\tau)(1-k)+(\gamma-\theta-\tau)H_\infty.$$

Assuming $1-k>0$ and $\gamma > \theta+\tau$, we look at conditions under which $\lambda_2 > 0$ and by rearranging the terms, we get $H_\infty > \dfrac{(\theta+\tau)(1-k)}{(\theta+\tau-\gamma)} = T$, where T is a negative threshold. Thus, all the biologically relevant equilibria on the line $(H_\infty, D_\infty) = (H_\infty, 0)$ are unstable. This is because H_∞ must be greater than or equal to $1-k$ in order for $\mathcal{P}[G] > 0$. For the remaining stability analysis of the non-isolated line of equilibria see Appendix A.

4.2 Local Stability Analysis of Healthy-Cell-Free Equilibrium

We analyze the stability of our isolated fixed point by first evaluating the Jacobian matrix at the equilibrium point $(H_\infty, D_\infty) = (0, 1-k)$ resulting in the following matrix:

$$J(0,1-k) = \begin{bmatrix} (\tau-\gamma)(1-k) & \tau(1-k) \\ (\gamma-\theta-\tau)(1-k) & -(\theta-\tau)(1-k) \end{bmatrix}.$$

This matrix produces the following two eigenvalues:

$$\lambda_1 = -\theta(1-k),$$

$$\lambda_2 = -\gamma(1-k).$$

Both θ and γ are positive by our given biological definition, therefore $(H_\infty, D_\infty) = (0, 1-k)$ is an asymptotically stable equilibrium point when $(1-k) > 0$. Under this condition:

$$k < 1,$$

$$2\mathcal{P}[G] + \mathcal{P}[S] < 1,$$

$$\text{at the initial state } \mathcal{P}[S]_0 = 0,$$

$$2\mathcal{P}[G]_0 < 1,$$

$$\mathcal{P}[G]_0 < \frac{1}{2}.$$

Thus, if the initial proportion of glial cells is less than half of the total proportion of cells, the proportion of healthy cells goes to zero. This result is expected because glial cells do not become damaged in our model, and help repair damaged cells to a healthy state and prevent further damage

from spreading.

4.3 Global Stability Analysis of Healthy-Cell-Free Equilibrium

Let $\mathcal{F}$ be defined as the biologically relevant state space of our dynamical system (refer to Figure 5). We do not consider regions outside of $\mathcal{F}$ because the given definitions of our state variables require that they are positive and $\mathcal{P}[D] + \mathcal{P}[H] \leq 1$. Also, $\mathcal{P}[D] + \mathcal{P}[H] \geq 1 - k$ for solutions to be biologically relevant, i.e. $\mathcal{P}[G] \geq 0$. Let $\partial\mathcal{F}$ denote the boundaries of $\mathcal{F}$. In order to show that trajectories do not diverge, we demonstrate that $\mathcal{F}$ is invariant under our two-dimensional dynamical system (meaning that trajectories inside $\mathcal{F}$ will remain inside $\mathcal{F}$ for all time). In order to do this we consider the vector flow on $\partial\mathcal{F}$ under the following conditions.

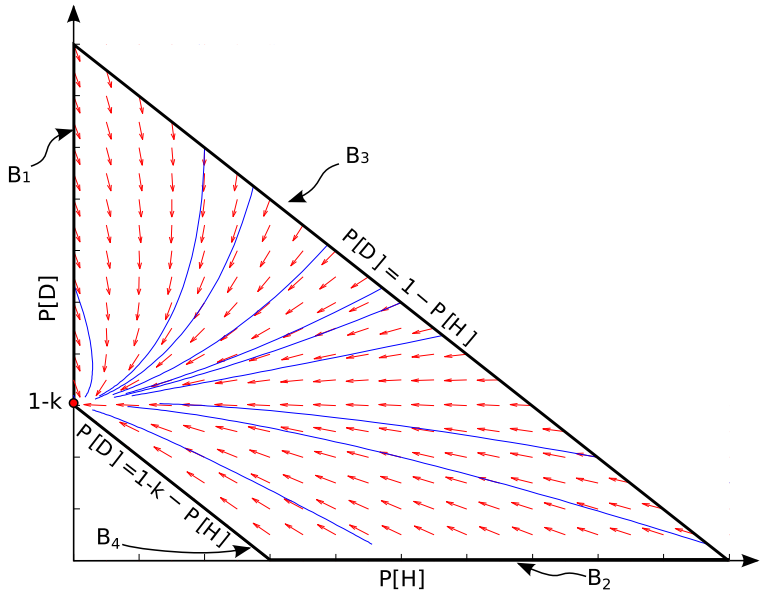

Figure 5: Vector flow with equilibrium point $(0, 1-k)$ within region $\mathcal{F}$

Consider the boundary $\mathcal{B}_1 = \{\partial\mathcal{F} : \mathcal{P}[H] = 0\}$. In order to remain within $\mathcal{F}$, $\frac{d}{dt}\mathcal{P}[H] = \mathcal{P}[D][\tau(\mathcal{P}[D] + k - 1)] \geq 0$. Given the condition $\mathcal{P}[D] \geq 1 - k$, it follows that $\frac{d}{dt}\mathcal{P}[H] \geq 0$.

Consider the second boundary $\mathcal{B}_2 = \{\partial\mathcal{F} : \mathcal{P}[D] = 0\}$. Then $\frac{d}{dt}\mathcal{P}[H] = 0$ and $\frac{d}{dt}\mathcal{P}[D] = 0$. Thus, the boundary $\mathcal{B}_2$ is a line of equilibria and solutions stay within our region.

Consider the third boundary $\mathcal{B}_3 = \{\partial\mathcal{F} : \mathcal{P}[H] + \mathcal{P}[D] = 1\}$ we want $\frac{d}{dt}\mathcal{P}[H] + \frac{d}{dt}\mathcal{P}[D] \leq 0$.

$$\begin{aligned}\frac{d}{dt}\mathcal{P}[H] + \frac{d}{dt}\mathcal{P}[D] &= -\theta(k - 1 + \mathcal{P}[H] + \mathcal{P}[D])\mathcal{P}[D], \\ &= -\theta k\mathcal{P}[D] \leq 0.\end{aligned}$$

This implies that our solutions cannot escape $\mathcal{F}$ through $\mathcal{B}_3$.

Finally, consider the fourth boundary $\mathcal{B}_4 = \{\mathcal{P}[D] + \mathcal{P}[H] = 1 - k\}$. We must show that $\frac{d}{dt}\mathcal{P}[D] + \frac{d}{dt}\mathcal{P}[H] \geq 0$.

$$\begin{aligned}\frac{d}{dt}\mathcal{P}[D] + \frac{d}{dt}\mathcal{P}[H] &= -\theta(k - 1 + \mathcal{P}[H] + \mathcal{P}[D])\mathcal{P}[D], \\ &= -\theta(k - 1 + (1 - k))\mathcal{P}[D] \geq 0.\end{aligned}$$

Thus, all solutions are bounded and remain within region $\mathcal{F}$ for all time.

The Dulac-Bendixson criterion is used to conclude there are no periodic orbits in the system, given that we find a suitable ϕ-function. A line of invariance exists at $\mathcal{P}[D] = 0$ due to the fact $\frac{d}{dt}\mathcal{P}[D] = 0$ when $\mathcal{P}[D] = 0$. Therefore, solutions that exist on the line ($\mathcal{P}[H]$, $\mathcal{P}[D]$) $= (H_\infty, 0)$ will remain on the line $(H_\infty, 0)$ for all time. Thus, the function $\phi = \frac{1}{\mathcal{P}[D]}$ is a suitable Dulac ϕ-function.

Applying Dulac's criterion:

$$\begin{aligned}&\frac{\partial}{\partial\mathcal{P}[D]}\left(\phi * \frac{d}{dt}\mathcal{P}[D]\right) + \frac{\partial}{\partial\mathcal{P}[H]}\left(\phi * \frac{d}{dt}\mathcal{P}[H]\right), \\ &= \frac{\partial}{\partial\mathcal{P}[D]}\left(\frac{1}{\mathcal{P}[D]} * \frac{d}{dt}\mathcal{P}[D]\right) + \frac{\partial}{\partial\mathcal{P}[H]}\left(\frac{1}{\mathcal{P}[D]} * \frac{d}{dt}\mathcal{P}[H]\right), \\ &= -\theta - \tau + \tau - \gamma = -(\theta + \gamma) < 0.\end{aligned}$$

This quantity remains negative for all values of $\mathcal{P}[D]$ and $\mathcal{P}[H]$, and thus by the Dulac-Bendixson criterion, there are no periodic solutions in the region $\mathcal{F}$. This fact in combination with the positive invariance of our region allows us to conclude that $(H_\infty, D_\infty) = (0, 1-k)$ is globally stable, when $1-k > 0$ and $\gamma > \theta + \tau$.

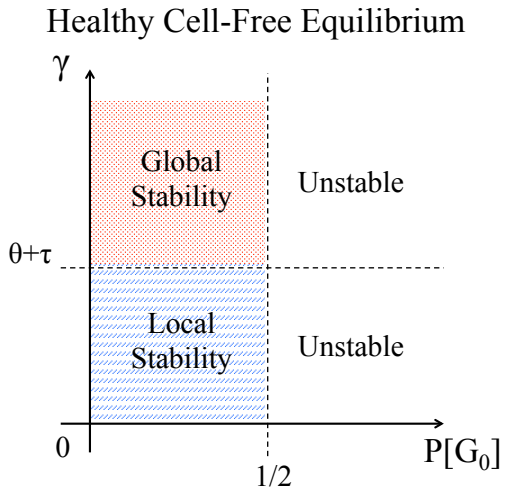

Figure 6: Healthy cell-free equilibrium parameter space

5 Pair Approximation Model

We use a pair approximation (OPA) model to analyze the impact of local spatial correlations on the dynamics of glial cell action after ischemic stroke. The OPA utilizes ordinary differential equations in a deterministic representation of the biological problem. However, it differs from the MFA in that it incorporates a degree of spatial dependence that is not seen by the latter. With the OPA, we can account for the effects of adjacency where the grid cell dynamics are not strongly influenced by non-adjacent cells. More specifically, we assume a Von Neumann neighborhood for these interactions. Consider an infinite lattice $\mathcal{L}$ with cells in states H, D, G, and S with no boundary. The state variables for the OPA are proportions of pairs of sites within the lattice, indicated by $\mathcal{P}[ij]$ where

$i, j \in \{H, D, G, S\}$. The pair $[ij]$ represents the spatial adjacency (cardinal neighbors) of the states i and j, and $\mathcal{P}[ij]$ is the proportion of pairs that are in the $[ij]$ configuration. All possible horizontal pair combinations are as follows:

[HH] [HD] [HG] [HS]

[DH] [DD] [DG] [DS]

[GH] [GD] [GG] [GS]

[SH] [SD] [SG] [SS]

Assuming rotational symmetry, $P[ij]$ is equivalent to $P[ji]$.

Of the 16 total state variables 6 exhibit rotational symmetry[1]. Therefore, only 10 state variables need to be explicitly derived. Furthermore, by the Law of Total Probability the 10th state variable can be written as 1 minus the sum of the other states, leaving only 9 state variables left to be explicitly derived[2].

The rate of change of $\mathcal{P}[ij]$ is the sum of all the rates of states changing into $[ij]$ minus the sum of the rates of $[ij]$ changing into other states:

$$\frac{d}{dt}\mathcal{P}[ij] = \sum inflow - \sum outflow$$

5.0.1 Construction of the OPA Model

The possible ways that states change are governed by the biological rules we have defined earlier. The respective OPA equations were derived using the above biological rules along with probability rules.

For example, the derivation of the rate of change in $\mathcal{P}$[HH] is outlined by the following steps:

[1] There are technically 32 pairs total due to vertical adjacency, 22 exhibit rotational symmetry

[2] The system can actually be reduced to 8 by using $2\frac{d}{dt}\mathcal{P}[G] + \frac{d}{dt}\mathcal{P}[S] = 0$

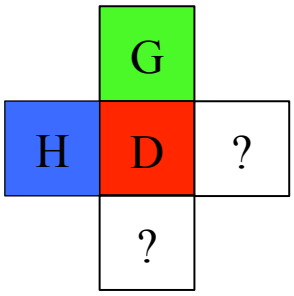

Figure 7: HD $\longrightarrow$ HH, given a G neighbor

- Identify all of the pairs that have the ability to change into the pair of interest with only one event occurring. In this case, the only pairs that can change into [HH] while following the biological rules we have outlined are [HD] and [DH] (since these states are the same by our assumption of rotational symmetry, they are simplified to $2\mathcal{P}$[HD]).

- The identified pairs are then multiplied by the corresponding rate(s) of the action that needs to be taken in order for the appropriate change to occur. For this example, τ is the appropriate parameter since it represents the rate of repair of a damaged cell into a healthy cell.

- Next, this expression is multiplied by the conditional probability of the acting cell being adjacent to the cell in question. In this example, the damaged cell can become a healthy cell only if it is adjacent to a glial cell, so the conditional probability that needs to be multiplied to the expression must be the probability of a G being adjacent to a D, given that we know the D is there.

- The final term to be multiplied to the expression is the fraction $\frac{3}{4}$: we know the identity of 1 neighbor of the given cell because we are working with pairs, therefore 3 neighbors are unknown and could possibly be the appropriate neighbor so we multiply by 3. Given that there is an appropriate neighbor, it has a $\frac{1}{4}$ chance to choose our given cell to act on so we

divide by 4.

This concludes the derivation of the inflow terms for $\mathcal{P}$[HH].

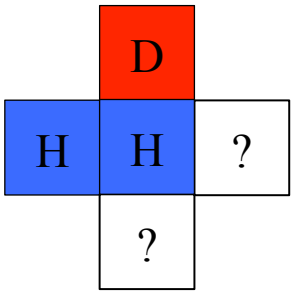

Figure 8: HH $\longrightarrow$ HD, given a D neighbor

The derivation of the outflow terms for $\mathcal{P}$[HH] uses the following logic:

- Identify all of the pairs which the pair of interest can change into. In this case [HH] can change only into [HD] and [DH], if we adhere to the biological rules we have defined.
- Identify the appropriate parameter that describes the rate of change for the particular action: γ describes the rate of change from H to D.
- Then the conditional probability is multiplied: In this case the conditional probability describes the chances of a D being adjacent to an H, given that the changing cell is an H (because damage to a healthy cell occurs only when a D is adjacent).
- The fraction $\frac{3}{4}$ must again be multiplied since 3 neighbors can be the appropriate one, with each neighbor having a $\frac{1}{4}$ chance to act on the cell of interest (D, in this case).

Putting the entire expression together, we come up with the following complete differential equation for $\mathcal{P}$[HH]:

$$\frac{dP[HH]}{dt} = 2P[HD]\left(\frac{3\tau P[DG]}{4P[D]}\right) - 2P[HH]\left(\frac{3\gamma P[HD]}{4P[H]}\right)$$

The same logic follows for the derivation of all the equations that comprise the OPA model:

$$\frac{d}{dt}\mathcal{P}[HH] = 2\mathcal{P}[HD]\left(\frac{3\tau\mathcal{P}[DG]}{4\mathcal{P}[D]}\right) - 2\mathcal{P}[HH]\left(\frac{3\gamma\mathcal{P}[HD]}{4\mathcal{P}[H]}\right)$$

$$\frac{d}{dt}\mathcal{P}[HG] = \mathcal{P}[DG]\left(\frac{3\tau\mathcal{P}[DG]}{4\mathcal{P}[D]} + \frac{\tau}{4}\right) - \mathcal{P}[HG]\left(\frac{3\theta\mathcal{P}[DG]}{4\mathcal{P}[G]} + \frac{3\gamma\mathcal{P}[HD]}{4\mathcal{P}[H]}\right)$$

$$\frac{d}{dt}\mathcal{P}[HD] = 2\mathcal{P}[DD]\left(\frac{3\tau\mathcal{P}[DG]}{4\mathcal{P}[D]}\right) + 2\mathcal{P}[HH]\left(\frac{3\gamma\mathcal{P}[HD]}{4\mathcal{P}[H]}\right) - \mathcal{P}[HD]\left(\frac{3\mathcal{P}[DG]}{4\mathcal{P}[D]}(\tau+\theta) + \frac{3\gamma\mathcal{P}[HD]}{4\mathcal{P}[H]} + \frac{\gamma}{4}\right)$$

$$\frac{d}{dt}\mathcal{P}[HS] = \mathcal{P}[DS]\left(\frac{3\tau\mathcal{P}[DG]}{4\mathcal{P}[D]}\right) + \mathcal{P}[HG]\left(\frac{3\theta\mathcal{P}[DG]}{4\mathcal{P}[G]}\right) + \mathcal{P}[HD]\left(\frac{3\theta\mathcal{P}[DG]}{4\mathcal{P}[D]}\right) - \mathcal{P}[HS]\left(\frac{3\gamma\mathcal{P}[HD]}{4\mathcal{P}[H]}\right)$$

$$\frac{d}{dt}\mathcal{P}[GG] = -2\mathcal{P}[GG]\left(\frac{3\theta\mathcal{P}[DG]}{4\mathcal{P}[G]}\right)$$

$$\frac{d}{dt}\mathcal{P}[GD] = \mathcal{P}[GH]\left(\frac{3\gamma\mathcal{P}[HD]}{4\mathcal{P}[H]}\right) - \mathcal{P}[GD]\left(\frac{3\theta\mathcal{P}[DG]}{4\mathcal{P}[D]} + \frac{\theta}{4} + \frac{3\mathcal{P}[DG]}{4\mathcal{P}[D]}(\tau+\theta) + \frac{\tau}{4}\right)$$

$$\frac{d}{dt}\mathcal{P}[GS] = \mathcal{P}[GD]\left(\frac{3\theta\mathcal{P}[DG]}{4\mathcal{P}[D]}\right) + \mathcal{P}[GG]\left(\frac{3\theta\mathcal{P}[DG]}{4\mathcal{P}[G]}\right) - \mathcal{P}[GS]\left(\frac{3\theta\mathcal{P}[GD]}{4\mathcal{P}[G]}\right)$$

$$\frac{d}{dt}\mathcal{P}[DS] = \mathcal{P}[DG]\left(\frac{3\theta\mathcal{P}[DG]}{4\mathcal{P}[G]}\right) + \mathcal{P}[DD]\left(\frac{3\theta\mathcal{P}[DG]}{4\mathcal{P}[D]}\right) + \mathcal{P}[HS]\left(\frac{3\gamma\mathcal{P}[HD]}{4\mathcal{P}[H]}\right) - \mathcal{P}[DS]\left(\frac{3\mathcal{P}[DG]}{4\mathcal{P}[D]}(\tau+\theta)\right)$$

$$\frac{d}{dt}\mathcal{P}[SS] = 2\mathcal{P}[GS]\left(\frac{3\theta\mathcal{P}[DG]}{4\mathcal{P}[G]}\right) + 2\mathcal{P}[DS]\left(\frac{3\theta\mathcal{P}[DG]}{4\mathcal{P}[D]}\right) + 2\mathcal{P}[GD]\left(\frac{\theta}{4}\right)$$

6 Numerical Results

The following results summarize how steady state conditions for H, D, G, and S vary with parameters θ and τ. We include three different sets of parameter sweeps for the CA for each initial

condition of damage dispersal (clustered, semi-clustered, and random). In addition to the parameter sweeps, steady states of each cell class are plotted with respect to the initial proportion of G.

D_∞ appears to be relatively constant for each CA parameter sweep set. Insights are difficult to derive from analysis of planar surfaces due to lack of variation, so we use the surface that describes the varying H_∞ with respect to θ and τ in order to determine optimal conditions for the parameters.

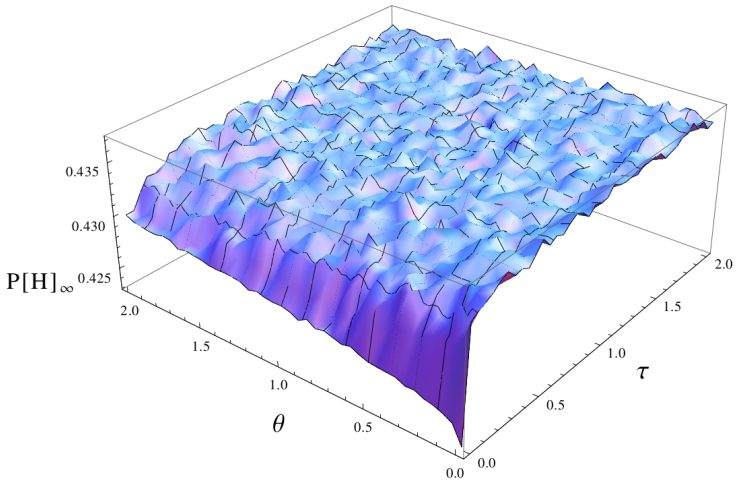

Figure 9: CA parameter sweep for clustered initial condition

H_∞ for the CA parameter sweep with clustered damage initial conditions (see Figure 9) seems to vary much more with alterations in τ rather than with alterations in θ when both parameters have small values. After a certain point, alterations in both parameters seem to have little effect. Values of the parameters have the most distinguished effect when the other parameter approaches 0.

The parameter sweep for H_∞ with semi-clustered damage dispersal exhibits a trend that varies more with different values of τ and θ than what was seen in the parameter sweep for clustered initial damage. This sweep also shows higher values of H_∞ when τ is favored over θ. Reference

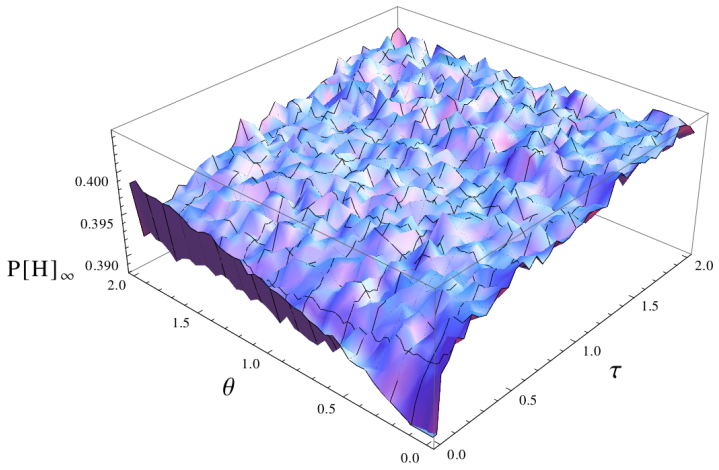

Figure 10: CA parameter sweep for semi-clustered initial condition

figure 10.

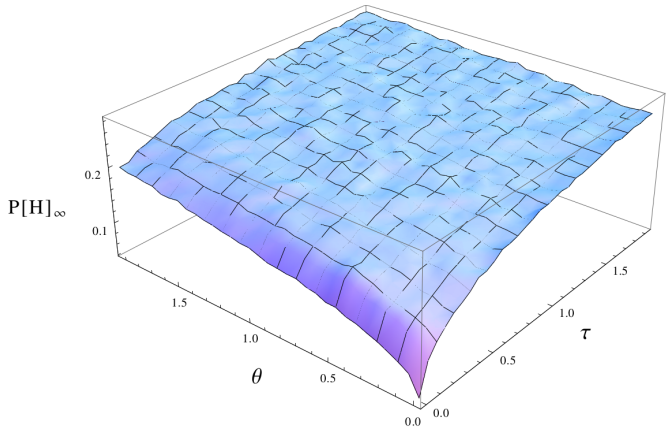

Figure 11: CA parameter sweep for random initial condition

The case for the CA parameter sweeps when initial damage is dispersed randomly is notably different than in both of the earlier cases (see Figure 11). θ alters the values seen for H_∞ moreso than in the semi-clustered and clustered damage cases, and highest values of H_∞ are observed when values of τ and θ are high. Though θ plays a larger role in this case compared to previous cases of initial conditions, τ still has the dominant role in this behavior.

Table 2 summarizes the range of steady states of our variables with varying initial conditions

Table 2: Steady State Min/Max in Varying θ and τ

	Clustered	Semi-Clustered	Random
H_∞	$42.4 - 43.7\%$	$38.8 - 40.4\%$	$0.0 - 26.0\%$
D_∞	$11.0 - 13.4\%$	$11.7 - 17.2\%$	$9.0 - 50.0\%$
G_∞	$42.0 - 44.0\%$	$44.0 - 41.5\%$	$14.0 - 44.0\%$
S_∞	$0.0 - 2.8\%$	$0.0 - 9.0\%$	$0.0 - 61.0\%$

of the CA. As the degree of randomness increases (from clustered to semi-clustered to random) the variance in the steady state ranges as well as the magnitude of damage and scarring increases.

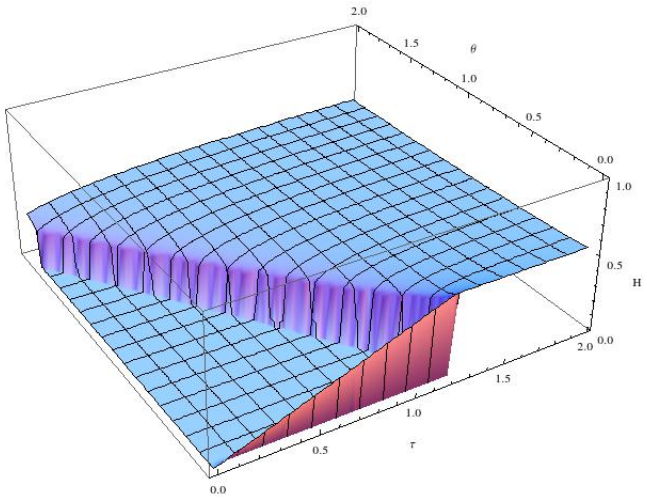

Figure 12: MFA parameter sweep

There are two distinct regions in the parameter sweep for each state variable in the MFA (see Figure 12). Each region is separated by a threshold involving θ and τ, giving pronounced differences in the predicted equilibrium values for our states. For combinations of θ and τ that are above the threshold, H_∞ and G_∞ are greater, whereas D_∞ and S_∞ are lesser. The situation is reversed when considering combinations of θ and τ that are below the threshold.

The parameter sweep for the case of OPA (see Figure 13) shows that H_∞ is affected more by θ than it is affected by τ, thus the case of OPA differs from the others in that significant changes in H_∞ are dictated more by θ rather than by τ.

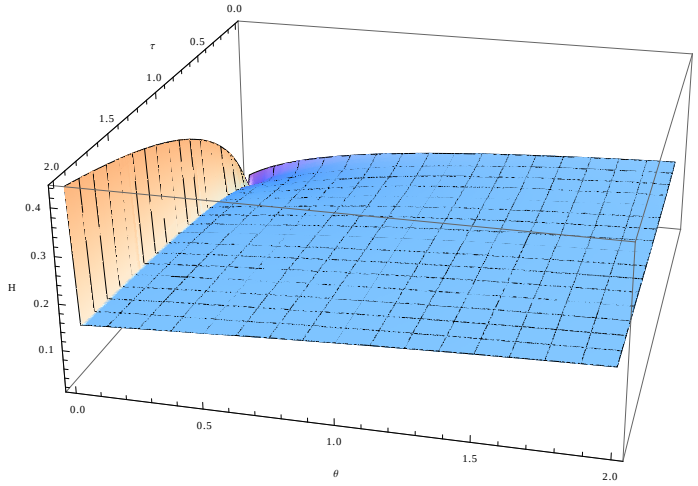

Figure 13: OPA parameter sweep

Figure 14 indicates that P[G_0] has a significant effect on the steady state values of all four variables, and this prediction by the CA is also supported by stability analysis performed on MFA. Certain initial proportions of P[G_0] give the highest values of H_∞. Higher values of G_0 decrease the values of D_∞ and S_∞ but lower H_∞ as well. This is due to the fact that we are using proportions and the total number of cells are conserved, therefore a linear increase in P[G_0] means a linear decrease in P[H_0].

7 Discussion

We use our parameter sweeps as a tool to identify relative tendencies of θ and τ that increase H_∞ while decreasing D_∞ and S_∞. As long as the rate of scar cell formation is greater than 0, it appears that scar cells will be great enough to contain the damage in all of the stochastic CA cases. After analysis of parameter sweeps, the effects of the initial proportions of G are interpreted.

The fact that H_∞ experiences greater increases with alterations in the rate of neural reparation

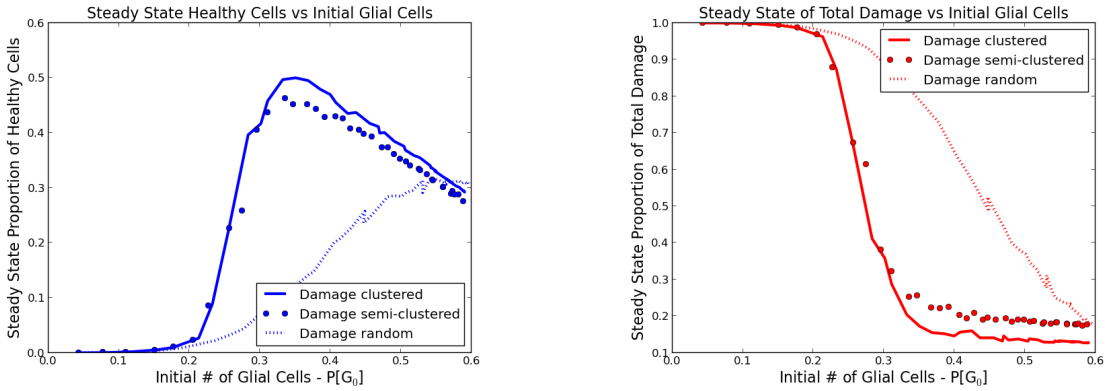

Figure 14: Effects of initial proportion of glial cells on: healthy cell steady state (left) and combined steady states of scar and damaged cells (right)

rather than with alterations in the rate of scar formation when both have small values suggests that treatment could be most beneficial if the rate of neural reparation is increased rather than the rate of scar cell formation, to a certain point.

The biological interpretation of H_∞ with respect to both the rate of neural reparation and the rate of scar cell formation in the case of semi-clustered damage dispersal in the CA suggests that H_∞ is more sensitive to changes in the rate of neural reparation rather than changes in the rate of scar formation. This supports the conclusion made from the CA parameter sweep with clustered initial damage.

In the case of randomly dispersed damage in the CA parameter sweep the rate of scar cell formation is more prominent in determining the value for H_∞ than in other CA parameter sweeps. Biologically, this means that scarring becomes more important when damage is dispersed more randomly. This is an effect of having a greater amount of contact between damaged cells and healthy and glial cells. Though the rate of scar cell formation has a larger role in this dispersal condition, the rate of neural reparation is still dominant and contributes more to increasing H_∞ than the rate of scar cell formation. This agrees with the other CA parameter sweeps.

Variance and breadth of injury increase with randomness. Spatial dependence limits the degree at which the dynamics can occur because it prohibits events from happening beyond a specific reactive interface. The reactive interface is defined by the region which glial and healthy cells are adjacent to damaged cells. The biological events that we have defined can only occur when those cells are next to each other. When the CA is more randomly distributed, there are more interfaces and the chance for damage to spread is high (as is the case for the OPA which is less spatially dependent and for the MFA which is not spatially dependent). In contrast, the CA simulation that is characterized by a clustered distribution of damage has a smaller interface. This is due to the fact that damaged cells that do not define the edge of a damaged area are not in contact with interactive cells and are therefore inert. The realization with a clustered distribution of damaged cells as well as the realization with random dispersal of damaged cells are not expected to be as accurate as the realization with a semi-clustered dispersal of damaged cells. This is due to the morphological architecture of blood vessels that supply the brain with oxygen.

The abrupt change in the equilibrium values of our state variables in the MFA parameter sweeps suggests a threshold of $\theta + \tau$. Combinations of the rate of scar cell formation and the rate of neural reparation that lay above this threshold are most beneficial for high proportions of healthy cells at steady state. Combined values of the rate of scar cell formation and the rate of neural reparation that are much higher than the threshold provide little benefit. In other words, after passing this threshold, beneficial increases in H_∞ diminish substantially. Biologically, there is little motivation to increase the values of the rate of scar cell formation and the rate of neural reparation if they are already above the threshold, though it may be favorable to pass the threshold by having larger values of the rate of neural reparation rather than having larger values of the rate of scar cell formation in order to increase H_∞. This is expected because having smaller values of the rate

of scar cell formation means consuming fewer glial cells for scar formation, thus conserving glial cells for neural repair. From this observation it may be favorable to administer treatment that increases neural reparation rather than scar tissue formation, given that the combination of glial cell activities passes the threshold observed in the MFA parameter sweeps.

In the case of the OPA, if there is any scar formation, ($\theta > 0$) the equilibrium values of all of our states drastically change: damaged, healthy, and glial cells drop while scar cells rise. This could possibly mean that the OPA system is so sensitive to scar formation that any non-zero value of the rate of scar cell formation will lead to large amounts of scar formation. Damage will be contained since healthy cells remain, but scar cells will comprise a very large proportion of brain tissue which is not favorable for functionality after recovery. Higher values of the rate of neural reparation can help offset the amount of scarring, but its contribution to changing equilibrium values is not as great as θ's, possibly indicating that the rate of scar cell formation is more important in overall brain health, while the rate of neural reparation serves as a supplement. This is in contrast to conclusions made from the MFA parameter sweeps, but correlates better with the case of the CA with randomly dispersed initial damage, which may be attributed to the OPA's unique degree of spatial dependence.

The initial proportion of G has a profound effect on the steady state values of the other variables. Increasing G_0 past a threshold decreases the amount of scarring, and there's a distinct value of G_0 that maximizes H_∞. Proportions of D_∞ and S_∞ that correspond to the maximum H_∞ can be brought down even lower while also making G_∞ higher, but only by sacrificing a higher proportion of H_∞. From these results it may prove beneficial to explore avenues that can alter the proportion of glial cells in the brain.

All scenarios of the CA parameter sweeps as well as the parameter sweep of the MFA suggest the rate of neural reparation plays a greater role than the rate of scar cell formation in granting functionality while containing damage. Consideration of the OPA offers an argument to that conclusion, although we expect that the CA models (semi-clustered in particular) are more reflective of the biology which inspired the question. Given that the rate of scar cell formation is not 0, we conclude that focusing treatment on neural reparation rather than scar cell formation may be more beneficial to brain health after stroke.

8 Future Work

Future work could include adding more complexity in the form of state variables. For example, expanding the glial cell state variable ($\mathcal{P}$[G]) into separate classes for the different types of glial cells (astrocytes, microglia, oligodendrocytes, etc.) may prove helpful in isolating type-specific actions that affect glial scar formation and neural repair. Adding even more state variables to describe other factors that come into play following a hypoxic event (oxygen concentration and dead cells for example) may provide a more accurate description of the trauma and resulting defensive actions.

We found that, in the stochastic CA model a correlation may exist between the degree of randomness of initial injury (D_0) and variance of total injury ($D_\infty + S_\infty$): variance in total injury increases as degree of initial randomness increases. However, we only analyze three points (completely random, semi-clustered, and completely clustered initial conditions). Future studies can help confirm the correlation we speculate by analyzing more points in the continuum of the degree of cluster. Furthermore, we suspect that a similar trend occurs between randomness and the breadth of injury, but more research is necessary.

Increasing the scope of this research project to include more complex events such as neurogenesis from neural stem cells following brain damage could provide results that are even more interesting and accurate. With the developments that take place within the theoretical and clinical realms, we can explore new methods to alter parameter values for neural repair and scar formation, possibly extending beyond the boundaries which our model has explored.

9 Acknowledgments

We would like to thank Dr. Carlos Castillo-Chavez, Executive Director of the Mathematical and Theoretical Biology Institute (MTBI), for giving us this opportunity to participate in this research program. We would also like to thank Co-Executive Summer Directors Dr. Omayra Ortega and Dr. Baojun Song for their efforts in planning and executing the day to day activities of MTBI. This research was conducted in MTBI at the Simon A. Levin Mathematical, Computational and Modeling Sciences Center (SAL MCMSC) at Arizona State University (ASU). This project has been partially supported by grants from the National Science Foundation (DMS-1263374 and DUE-1101782), the National Security Agency (H98230-14-1-0157), the Office of the President of ASU, and the Office of the Provost of ASU.

References

[1] Pierre Brémaud. *Markov chains : Gibbs fields, Monte Carlo simulation and queues.* Texts in applied mathematics. Springer, New York, Berlin, Heidelberg, 1999.

[2] Valerie Cheathon, Agustin Flores, Victor Suriel, Octavious Talbot, Dustin Padilla, Marta Sarzynska, Adrian Smith, and Luis Melara. Dynamics and Control of an Invasive Species: The Case of the Rasberry Crazy Ant Colonies. Technical Report MTBI-10-03M, Arizona State University, Tempe, July 2013.

[3] Joanne O Davidson, Colin R Green, Laura Bennet, Louise F B Nicholson, Helen Danesh-Meyer, Simon J O'Carroll, and Alistair J Gunn. A key role for connexin hemichannels in spreading ischemic brain injury. *Current Drug Targets*, 14(1):36–46, January 2013.

[4] M Angels Font, Adriá Arboix, and Jerzy Krupinski. Angiogenesis, neurogenesis and neuroplasticity in ischemic stroke. *Current cardiology reviews*, 6(3):238–244, August 2010.

[5] Alan S Go, Dariush Mozaffarian, Véronique L Roger, Emelia J Benjamin, Jarett D Berry, Michael J Blaha, Shifan Dai, Earl S Ford, Caroline S Fox, Sheila Franco, Heather J Fullerton, Cathleen Gillespie, Susan M Hailpern, John A Heit, Virginia J Howard, Mark D Huffman, Suzanne E Judd, Brett M Kissela, Steven J Kittner, Daniel T Lackland, Judith H Lichtman, Lynda D Lisabeth, Rachel H Mackey, David J Magid, Gregory M Marcus, Ariane Marelli, David B Matchar, Darren K McGuire, Emile R Mohler, Claudia S Moy, Michael E Mussolino, Robert W Neumar, Graham Nichol, Dilip K Pandey, Nina P Paynter, Matthew J Reeves, Paul D Sorlie, Joel Stein, Amytis Towfighi, Tanya N Turan, Salim S Virani, Nathan D Wong, Daniel Woo, and Melanie B Turner. Heart Disease and Stroke Statistics—2014 Update: A Report From the American Heart Association. *Circulation*, 129(3):e28–e292, January 2014.

[6] Corinna Haupt, Otto W Witte, and Christiane Frahm. Up-regulation of Connexin43 in the glial scar following photothrombotic ischemic injury. *Molecular and Cellular Neuroscience*, 35(1):89–99, January 2007.

[7] David E. Hiebeler and Benjamin R. Morin. The effect of static and dynamic spatially structured disturbances on a locally dispersing population. *Journal of Theoretical Biology*, 246(1):136 – 144, 2007.

[8] Rong Hu, Jianjun Zhou, Chunxia Luo, Jiangkai Lin, Xianrong Wang, Xiaoguang Li, Xiuwu Bian, Yunqing Li, Qi Wan, Yanbing Yu, and Hua Feng. Glial scar and neuroregeneration: histological, functional, and magnetic resonance imaging analysis in chronic spinal cord injury. *Journal of Neurosurgery: Spine*, 13(2):169–180, January 2014.

[9] Lijie Huang, Zhe-Bao Wu, Qichuan Zhuge, Weiming Zheng, Bei Shao, Brian Wang, Fen Sun, and Kunlin Jin. Glial scar formation occurs in the human brain after ischemic stroke. *International journal of medical sciences*, 11(4):344–348, January 2014.

[10] Jeffrey L Saver. Time Is Brain—Quantified. *Stroke*, 37(1):263–266, January 2006.

[11] Neil R Sims and Hakan Muyderman. Mitochondria, oxidative metabolism and cell death in stroke. *Biochimica et Biophysica Acta (BBA) - Molecular Basis of Disease*, 1802(1):80–91, January 2010.

10 Appendix A

Previously, we determined that $(H_\infty, D_\infty) = (H_\infty, 0)$ is an equilibrium point in our two-dimensional system in our Mean-Field model. The Jacobian matrix evaluated at $(H_\infty, D_\infty) = (H_\infty, 0)$ is:

$$J(H^*, 0) = \begin{bmatrix} 0 & \tau(1-k) + (\tau - \gamma)H_\infty \\ 0 & (\theta + \tau)(1-k) + (\gamma - \theta - \tau)H_\infty \end{bmatrix}.$$

This matrix had produced the following eigenvalues λ_1 and λ_2:

$$\begin{cases} \lambda_1 = 0 \\ \lambda_2 = (\theta + \tau)(1-k) + (\gamma - \theta - \tau)H_\infty \end{cases}$$

During our initial analysis of the stability of this equilibrium point under the condition that $D + H \geq 1 - k$, we made the two assumptions $1 - k > 0$ and $\gamma > \theta + \tau$. We can do further analysis with three assumptions: an assumption that $1 - k < 0$ and $\gamma < \theta + \tau$, an assumption that $1 - k > 0$ and $\gamma < \theta + \tau$, and an assumption that $1 - k < 0$ and $\gamma > \theta + \tau$.

10.1 Case 1

First, consider the case where $1 - k < 0$ and $\gamma < \theta + \tau$. We can then attempt to find a threshold in which our value of H_∞ would change the sign of our second eigenvalue λ_2, and therefore the equilibrium point's stability. We initially assume that the second eigenvalue λ_2 is positive, therefore generating an unstable equilibrium point. By manipulating the equation of the second eigenvalue λ_2 under the assumption that it is positive, we derive the following stability threshold:

$$H_\infty < \frac{(\theta + \tau)(1-k)}{-(\gamma - \theta - \tau)}$$

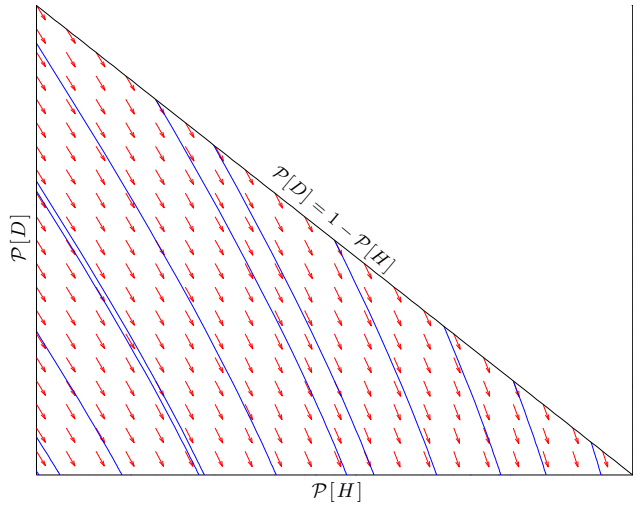

Figure 15: Phase plane depicting Case 1

We know $\theta > 0$ and $\tau > 0$ given our biological definition, therefore $(\theta + \tau) > 0$. Because we assumed $1 - k < 0$ and $\gamma < \theta + \tau$, it holds true that our threshold value is less than zero. this means that the equilibrium point under these conditions is unstable if and only if $H_\infty < 0$, which is not biologically possible. Therefore, for all biologically significant values of H_∞, the equilibrium $(H_\infty, D_\infty) = (H_\infty, 0)$ is stable under these conditions.

10.2 Case 2

Next, consider the case where $1 - k > 0$ and $\gamma < \theta + \tau$. We can then attempt to find a threshold in which our value of H_∞ would change the sign of our second eigenvalue λ_2, and therefore the equilibrium point's stability. We initially assume that the second eigenvalue λ_2 is positive, therefore generating an unstable equilibrium point. By manipulating the equation of the second eigenvalue

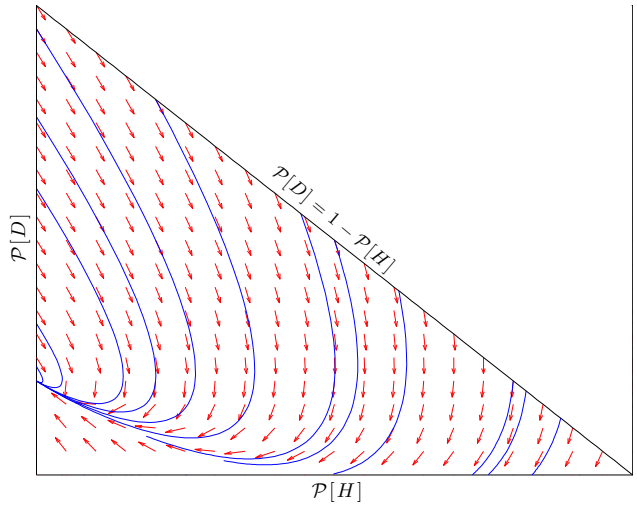

Figure 16: Phase plane depicting Case 2

λ_2 under the assumption that it is positive, we derive the following stability threshold:

$$H_\infty < \frac{(\theta + \tau)(1 - k)}{-(\gamma - \theta - \tau)} = \mathcal{T}_1$$

We know $\theta > 0$ and $\tau > 0$ given our biological definition, therefore $(\theta + \tau) > 0$. Because we assumed $1 - k > 0$ and $\gamma < \theta + \tau$, our threshold value is greater than zero, which is biologically possible. Due to our assumption on the initial sign of our eigenvalue λ_2, the equilibrium point is unstable if $H_\infty < \mathcal{T}_1$. The equilibrium point is stable if $H_\infty > \mathcal{T}_1$.

10.3 Case 3

Lastly, consider the case where $1 - k < 0$ and $\gamma > \theta + \tau$. We can then attempt to find a threshold in which our value of H_∞ would change the sign of our second eigenvalue λ_2, and therefore the equilibrium point's stability. We initially assume that the second eigenvalue λ_2 is positive, therefore

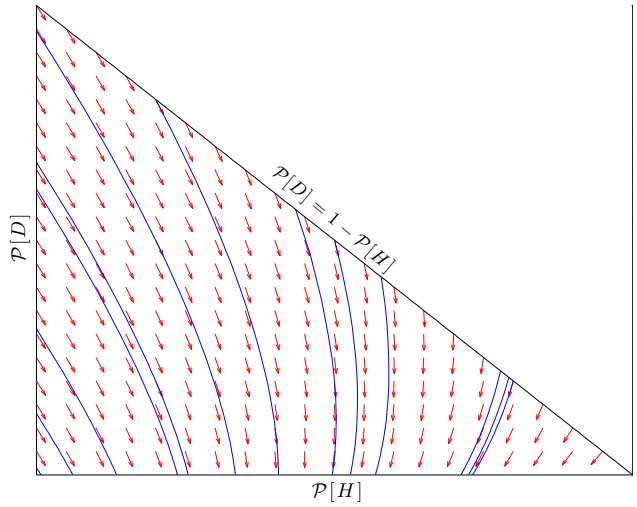

Figure 17: Phase plane depicting Case 3

generating an unstable equilibrium point. By manipulating the equation of the second eigenvalue λ_2 under the assumption that it is positive, we derive the following stability threshold:

$$H_\infty > \frac{(\theta + \tau)(1 - k)}{-(\gamma - \theta - \tau)} = \mathcal{T}_2$$

We know $\theta > 0$ and $\tau > 0$ given our biological definition, therefore $(\theta + \tau) > 0$. Because we assumed $1 - k < 0$ and $\gamma > \theta + \tau$, our threshold value is greater than zero, which is biologically possible. Due to our assumption on the initial sign of our eigenvalue λ_2, the equilibrium point is unstable if $H_\infty > \mathcal{T}_2$. The equilibrium point is stable if $H_\infty < \mathcal{T}_2$.